



# Comparison of probabilistic models for stress rupture failure in continuous unidirectional fiber composite structures

Amy Engelbrecht-Wiggans<sup>1,\*</sup>  and Stuart Leigh Phoenix<sup>1</sup> 

<sup>1</sup> Mechanical and Aerospace Engineering, Cornell University, 321 Thurston, Ithaca, NY 14853, USA

**Received:** 17 June 2017

**Accepted:** 1 February 2018

**Published online:**  
12 February 2018

© Springer Science+Business Media, LLC, part of Springer Nature 2018

## ABSTRACT

Stress rupture is an important failure phenomenon in composite overwrapped pressure vessels, which is highly unpredictable other than on a statistical basis. Even then, there are several statistical models, with varying bases in composite micromechanics and molecular failure mechanisms. Choosing among these models is not trivial, even when micromechanical details of the failure process are reasonably well appreciated, and one has available a reasonably large database of strength and lifetime data. As a result, there is little in the way of guidance to choose the most appropriate model. One important issue is that accurate predictions are desired at relatively low service loads compared to the strength, and low probabilities of failure that are far less, e.g.,  $10^{-6}$ , than can be directly confirmed using the data itself. In essence, one needs a robust and accurate statistical model free of inconsistencies associated with such low stress levels and probabilities of failure. This paper performs an in-depth comparison of several current models, which have varying physical bases. The models compared differ in the number of parameters to be estimated from data. The results of this study, however, show that over a broad range of parameter values these models give surprisingly similar failure probability predictions. While practitioners may have a preference for one model over another, the basis for such a choice is not easily established, given the fidelity of typical data.

## Introduction

Stress rupture is a long-term, catastrophic failure mode in unidirectional continuous fiber composites. Stress rupture failures happen suddenly, with little to no warning, and at present eminent failures cannot be reliably predicted with nondestructive evaluation.

Stress rupture occurs at normal operating temperatures and at load levels well below the initial failure load, though stress rupture failures will occur sooner with increased temperature and/or load. Examples of unidirectional continuous fiber composites susceptible to stress rupture are composite overwrapped pressure vessels (COPVs), composite flywheels for

Address correspondence to E-mail: aee52@cornell.edu

energy storage, and long tension members used in civil engineering structures. For COPVs in particular, stress rupture failures are of increasing concern as COPVs are being designed with longer service lives and higher service pressures in mind. Also, the number of COPVs in use is rapidly growing, so even though a stress rupture failure may be a relatively low probability event, we can anticipate seeing such failures in applications if stress rupture is not properly understood and accounted for.

Stress rupture failures develop from the randomly distributed flaws that are inherent in any fiber. This causes not only an intrinsic randomness in the fiber strength, including a size effect, but also intrinsic randomness in the strength of corresponding unidirectional continuous fiber composites. Thus, the exact strength of a composite specimen cannot be known in advance. Because of this intrinsic randomness, the exact failure time of a specimen also cannot be known ahead of time. At best, the overall stress rupture behavior for a population of identical specimens must be statistically characterized. From extensive testing as well, as theory, we know that the failure strength is very close to Weibull distributed. The lifetimes under a constant load are also approximately Weibull distributed. A probabilistic model can then be used to relate lifetimes at different loads to each other, as well as to initial strength.

The goal of this paper is to compare various models that have arisen in the literature. In particular, this paper compares what is referred to as (1) the 1979 functional form [1], (2) the classic power-law model [2–8], (3) the crack-growth model [9, 10], and (4) the strength decay model [11], all of which are cast in a power-law Weibull framework.

## Motivation

A primary motivation for the study in this paper is that the four models considered have been used variously to forecast the reliable lifetime of composite structures, such as composite overwrapped pressure vessels (COPVs) used in aerospace and other transportation settings [11–17]. Practitioners in industry and at government laboratories tend to settle on one of these simple models, and even to have a favorite, which they believe is somehow more realistic than another model. For instance, the model based on Paris-law crack-growth principles in a Weibull

framework might seem preferable as having a strong basis in mechanics.

A second motivation for this study is that even if two models seem to have almost the same basic behavior, the particular choice of one model over another matters in practice. The various models have differing numbers of parameters that also differ subtly in their effects on the probability distributions for failure, particularly in the extreme lower tails. This is important since reliability requirements may be very high, i.e., less than one failure in ten million. Thus, it is important to understand how the models differ in the tails, under certain types of loadings and over practically important parameter ranges, before committing to one model versus another. Note that while these models do differ in the deep lower tails for lifetime, it is unlikely that such differences would be apparent even in the largest datasets.

In principle, having more parameters allows for more flexibility in fitting the model to experimental data. Unfortunately, having more parameters also means that the uncertainty will be larger in each parameter estimate as well as the uncertainty for any failure probability prediction, at a given stress level and a desired service lifetime. Furthermore, generating additional data to reduce this uncertainty may be impractical. All other things being nearly equal, the model with the fewest fitting parameters will have the least uncertainty in lifetime predictions.

## Experimental datasets

With respect to the behavior of the various models when compared to experimental data on resin impregnated strands or larger composite structures, it would certainly be desirable to have extensive databases on both strength and stress rupture lifetime of such structures to inform choosing a particular model and to make predictions. While some databases do exist, on closer scrutiny the actual data in them are often fraught with omissions (failure to record certain data believed somehow to be illegitimate), undocumented censoring issues and other confounding factors. Running tests that take months, or even years, is fraught with problems, such as equipment or power failures, personnel turnover and changes in management priorities, and even the occurrence of earthquakes, all of which can compromise the integrity of the data, particularly with

respect to validating model behavior in the lower and upper tails of interest in this paper.

Regarding the general features of datasets, strength data are typically Weibull in behavior, and apparent non-Weibull behavior can simply be the result of having a limited sample size, or, be a reflection of clamping or loading problems. There may also be outliers in the data caused by such things as a technician mishandling a few specimens when mounting them for testing. While some strength datasets may appear to have non-Weibull features, these features are often not repeatable, i.e., components or resin impregnated strands made from other fiber spools from the same lot may not exhibit the same non-Weibull features. That said, the vast majority of strength datasets are acceptably Weibull.

With respect to lifetime under constant load, complete lifetime datasets that are detailed enough to establish non-Weibull features, particularly in the tails, are rare. At the outset, lifetime testing is costly, and most lifetime datasets that pass scrutiny are not large enough to definitively establish whether or not there are significant non-Weibull features. Most datasets are censored in their upper tails since there is insufficient time available to run the tests to completion, particularly at lower load levels (though still above service load). Thus, the existence of non-Weibull behavior in the upper tails is difficult to establish experimentally.

When non-Weibull features are seemingly observed in the lower tails, one must first determine whether such data have been subtly filtered. For instance, in lifetime experiments under constant load it may happen that the data in the lower tails have been ‘truncated,’ which refers to the inappropriate discarding of data associated with failures that occur when initially ramping up the load. In these cases, it is assumed that such specimens were somehow faulty, yet according to the strength distribution a certain number of such failures should have been expected. Unfortunately, such practices lead to inconsistency in the datasets that greatly increase the uncertainty in failure probability predictions.

### Size scaling

The ability to do size scaling is also an important issue since one would very much like to use test data from less costly, small-scale composite specimens to predict the strength and lifetime behavior of much

larger scale components (by orders of magnitude), that are likely to be tested in very small numbers, at best. For instance, in qualifying a COPV design for service, some test standards require performing only one burst test, or perhaps two, and obviously this does not provide meaningful statistics. Thus, one is left making forecasts based on using whatever data happen to be available from smaller-scale specimens, such as epoxy-impregnated strands (yarns or tows) that may not even use the same epoxy. For many material systems, there is only limited data available, and one needs to select a model carefully and have parameter estimation methods that will make the best use of it.

The Weibull lifetime shape parameter,  $\beta$ , which is discussed later in “[Probabilistic models](#)” section and is roughly inversely proportional to the variability in lifetime, may well increase with the size of the composite structure (causing the variability to decrease). However, experimental data with enough resolution to demonstrate this phenomenon are sparse and often fraught with confounding factors. For instance, one must be careful to account for small sample bias in maximum likelihood estimates of  $\beta$ , which tend to inflate the value. This is important as the larger the composite structure, the fewer the number of specimens that tend to be tested. Based on the theory discussed in “[Micromechanics-based stochastic models](#)” section, one might expect (and practitioners will hope for) a larger  $\beta$  value as the composite structure size increases. Nonetheless, while we have accommodated size scaling in the model, one should still be cautious in assuming such size scaling will apply beyond more than one or two orders of magnitude.

### Micromechanics-based stochastic models

Regarding more sophisticated, micromechanically based, stochastic models, there has been much progress made in developing fiber bundle-based models for composite strength and lifetime under various idealized assumptions on stress redistribution from broken to surviving fibers. While these models provide considerable insight into composite failure phenomena, they are not yet used in practice as engineers favor the much simpler versions studied in this paper.

These more advanced models, as well as those in this paper, do not go far enough in answering certain

critical questions such as ‘When is a proof-test stress level too high, to the point of doing more harm than good later in the lifetime of the vessel?’ For instance, the model based on Paris-law crack growth of initial, randomly distributed flaws or cracks of various sizes implies there is no such thing as ‘too high’ for a proof test (other than perhaps destroying perfectly good composite components). In this model, flaws are assumed to grow negligibly during a proof test, and therefore, any flaw or crack weeded out is a good thing, since it is also assumed that no new flaws are created. All the models we consider have this same optimistic reliability improvement at all future times after a proof test, particularly for carbon/epoxy composites.

Such permanent life enhancement, however, may not be realistic in a COPV, particularly one made of carbon fibers proof-tested to more than three quarters of its burst strength. The time-dependent, creep-rupture mechanism in a composite structure stems largely from matrix creep in shear and/or time-dependent, debonding and slip around fiber breaks that over time increases the length-scale of fiber-to-fiber load transfer. This exposes additional fiber flaws, which also subsequently result in fiber breaks. There is no question—as is clear from knowledge of the fiber strength distribution and acoustic emission generated—that excessive proof testing results in broken fibers that otherwise would not have occurred at service load levels. These now become seeds for the growth of new break clusters. This last aspect of proof-test-induced damage was the rationale behind a model called the fiber breakage model, originally developed in [18]. The current authors are continuing work on this model and calculations thus far confirm that, after a brief ‘safe time,’ the failure probability at longer times can quickly become worse than for the case where a minimal proof test has been performed.

## Probabilistic models

The earliest of the existing probabilistic models to describe stress rupture failures date from the 1940s and 1950s [2–6]. These models tend to have a more phenomenological than micromechanics basis, though some are well based in the molecular failure processes for a single fiber [7, 8].

In the literature, there are currently three specific probabilistic models, each a parametric variation of a

general functional form. The oldest and most commonly used is the classic power-law model in a Weibull framework (CPL-W) [5, 19, 20]. Another model is based on Paris-law crack growth, termed the crack-growth model [9, 10, 21]. The most recent model is the strength decay model [11].

## 1979 Functional form

Many of the currently existing models fit into the functional form proposed by Phoenix in 1979 [1]:

$$F(t|\sigma) = \sup_{0 \leq \tau \leq t} \{\psi(\sigma(\tau), Z(\tau; \sigma(\tau)))\}. \quad (1)$$

here  $\psi(\sigma, Z)$  is the shape function in terms of the nonnegative stress profile,  $\sigma(t)$ ,  $t \geq 0$ , where  $Z$  provides for the introduction of degradation over time. Equation (1) was actually proposed for single fiber behavior as an assumption in modeling bundle lifetime.

A useful shape function for stress rupture is:

$$\psi(\sigma, Z(\tau; \sigma(\tau))) = 1 - \exp\left\{-\left(\left(\frac{\sigma}{\sigma_{\text{ref}}}\right)^r + \frac{Z(\tau; \sigma(\tau))}{t_{\text{ref}}}\right)^\beta\right\}, \quad (2)$$

where  $\sigma_{\text{ref}}$  is a stress scaling parameter,  $t_{\text{ref}}$  is a time scaling parameter,  $\beta$  is the shape parameter, and  $r$  is a parameter reflecting the sensitivity of the material to instantaneous load.

A useful degradation form, reminiscent of Miner’s rule [22], takes the integral structure

$$Z(\tau; \sigma(\tau)) = \int_0^\tau \kappa(\sigma(s)) ds \quad (3)$$

where  $\kappa(\sigma)$  is the breakdown rule. Most current models for stress rupture use a power-law breakdown rule [23], with molecular justification in terms of thermal activation processes in [5, 24–26]:

$$\kappa(\sigma(t)) = \left(\frac{\sigma(t)}{\sigma_{\text{ref}}}\right)^\rho, \quad \sigma(t) \geq 0, \quad (4)$$

where  $\rho$  is the power-law exponent, controlling sensitivity to variations in the applied stress. Some more recent modeling of stress rupture in fiber systems, using the power-law breakdown rule, is presented in [12, 13].

An alternative is the exponential breakdown rule, with a long history beginning with Coleman [2, 3] and Zhurkov [27]:

$$\kappa(\sigma(t)) = \mu \exp\left\{\frac{\sigma(t)}{\sigma_{\text{ref}}}\right\}, \quad \sigma(t) \geq 0, \tag{5}$$

where  $\mu$  is a scaling constant. In many circumstances, (4) and (5) are equally realistic in modeling experimental datasets [20], and with properly chosen parameters both rules give qualitatively similar results [23]. There are some circumstances where (5) may be more accurate, such as in [28], however, (5) has significant drawbacks mathematically [24].

Combining (1), (2), (3) and (4) gives the form of (1) that is most applicable to stress rupture in composites:

$$F_{1979}(t|\sigma) = 1 - \exp\left\{- \sup_{0 \leq \tau \leq t} \left\{ \left[ \left( \frac{\sigma(\tau)}{\sigma_{\text{ref}}} \right)^r + \int_0^\tau \left( \frac{\sigma(s)}{\sigma_{\text{ref}}} \right)^\rho \frac{ds}{t_{\text{ref}}} \right]^\beta \right\} \right\}, \quad t \geq 0 \tag{6}$$

This is the version of the functional form that will be considered for the rest of the paper.

In the case of strength testing, the stress is assumed to be linearly increasing:

$$\sigma(t) = Rt, \quad t \geq 0 \tag{7}$$

where the constant,  $R > 0$ , is the loading rate or stress rate. Under this load profile, (6) simplifies to the cumulative distribution function for failure stress in a strength test:

$$F_{1979,s}(s) = 1 - \exp\left\{- \left[ \left( \frac{s}{\sigma_{\text{ref}}} \right)^r + \left( \frac{s}{\sigma_{\text{ref}}} \right)^\rho \frac{s}{Rt_{\text{ref}}(\rho + 1)} \right]^\beta \right\} \tag{8}$$

where  $s = Rt > 0$  is the stress level at failure.

In the case of stress rupture lifetime testing, the load is held constant:

$$\sigma(t) = \bar{\sigma}, \quad t > 0 \tag{9}$$

Using (9), the cumulative distribution function for time to failure simplifies from (6) to:

$$F_{1979,\bar{\sigma}}(t) = 1 - \exp\left\{- \left[ \left( \frac{\bar{\sigma}}{\sigma_{\text{ref}}} \right)^r + \left( \frac{\bar{\sigma}}{\sigma_{\text{ref}}} \right)^\rho \frac{t}{t_{\text{ref}}} \right]^\beta \right\} \tag{10}$$

Thus, the functional form can be given in general by (6), with a strength distribution given by (8) and a lifetime distribution given by (10). The 1979 functional form has five parameters:  $\sigma_{\text{ref}}$ ,  $r$ ,  $\rho$ ,  $\beta$ , and  $t_{\text{ref}}$ .

Changing the type of material is likely to change the relationship between  $r$  and  $\rho$ . A material with a large  $r$ , respective to  $\rho$ , would have an almost deterministic strength distribution for extremely high loading rates; however, at slow loading rates the strength distribution has greatly increased variability. This might be the case where flaws of uniform size inherently grow at differing rates. In contrast, a material with a small  $r$ , respective to  $\rho$ , would have more variability in the strength distribution at extremely high loading rates than at slow ones. This might be the case where the flaws themselves are highly variable, but grow in a way that ultimately masks the initial variability. This paper will consider  $-4 \leq r - \rho \leq 32$  in order to illustrate the differences between models, whether or not these values correspond specifically to a particular material.

To adapt the 1979 functional form, or indeed any of the probabilistic models discussed, for size scaling, a volume term can be added:

$$F_{1979}(t|\sigma) = 1 - \exp\left\{- \frac{V}{V_{\text{ref}}} \sup_{0 \leq \tau \leq t} \left\{ \left[ \left( \frac{\sigma(\tau)}{\sigma_{\text{ref}}} \right)^r + \int_0^\tau \left( \frac{\sigma(s)}{\sigma_{\text{ref}}} \right)^\rho \frac{ds}{t_{\text{ref}}} \right]^\beta \right\} \right\}, \quad t \geq 0 \tag{11}$$

where  $V$  is the desired volume, and  $V_{\text{ref}}$  is a volume for which the other material parameters, i.e.,  $\sigma_{\text{ref}}$ ,  $r$ ,  $\rho$ ,  $\beta$ , and  $t_{\text{ref}}$ , are known from experimental data. [17] Henceforth, to simplify the notation, we will omit the volume factor,  $V/V_{\text{ref}}$ , with the understanding that this can always be inserted following the negative sign in the exponential.

### Classic power-law model in a Weibull framework (CPL-W)

The CPL-W model was developed to describe the behavior of a single fiber, but is generally applied to the whole composite structure. CPL-W is mostly phenomenological, though a molecular basis has been established: it has been shown that the model is a consequence of the Tobolsky–Eyring theory of thermally activated bond breakage [5, 24, 25, 29]. The CPL-W model fits strength and lifetime data well, albeit with some small differences in comparison with data in the tails of the distribution, in which the CPL-W model happens to be conservative. Seeing

these differences likely requires very large sample sizes (in the hundreds) [29].

The probability of failure of a specimen in stress rupture is given by the CPL-W model to be:

$$F_{\text{CPL-W}}(t|\sigma) = 1 - \exp \left\{ - \left[ \int_0^t \left( \frac{\sigma(\tau)}{\sigma_{\text{ref}}} \right)^\rho \frac{d\tau}{t_{\text{ref}}} \right]^\beta \right\} \quad (12)$$

where  $\rho$  is the power-law exponent, controlling sensitivity to changes in the applied stress,  $\sigma_{\text{ref}}$  is a stress scaling parameter,  $t_{\text{ref}}$  is a time scaling parameter, and  $\beta$  is the Weibull scale parameter, as before in (2) and (4), and as above we have omitted reference to the volume factor,  $V/V_{\text{ref}}$ , with the understanding that it can always be inserted following the negative sign in the exponential. Note that (12) can be written as

$$F_{\text{CPL-W}}(t|\sigma) = 1 - \exp \left\{ - \left[ \frac{1}{\sigma_{\text{ref}}^\rho t_{\text{ref}}} \int_0^t \sigma(\tau)^\rho d\tau \right]^\beta \right\} \quad (13)$$

so that there is only one scale parameter, namely  $\sigma_{\text{ref}}^\rho t_{\text{ref}}$ , albeit an unintuitive one with inconvenient dimensions. Nonetheless, the importance of Eq. (13) is that the four parameters shown in (12) are not independent. Instead, there is a relationship between  $\sigma_{\text{ref}}$ ,  $t_{\text{ref}}$  and  $\rho$ , such that  $\sigma_{\text{ref}}^\rho t_{\text{ref}}$  is a constant for a given material.

Applying the model, (12), to the case of strength testing, the cumulative distribution function for failure stress becomes:

$$F_{\text{CPL-W},s}(s) = 1 - \exp \left\{ - \left[ \left( \frac{s}{\sigma_{\text{ref}}} \right)^\rho \frac{s}{R t_{\text{ref}} (\rho + 1)} \right]^\beta \right\} \quad (14)$$

where again  $s = Rt$  is the stress level at failure. This can be written as

$$F_{\text{CPL-W},s}(s) = 1 - \exp \left\{ - \left( \frac{s}{\sigma_{\text{ref}}} \right)^{\beta(\rho+1)} \right\} \quad (15)$$

by assuming

$$\sigma_{\text{ref}} = R t_{\text{ref}} (\rho + 1) \quad \text{or} \quad t_{\text{ref}} = \frac{\sigma_{\text{ref}}}{R(\rho + 1)} \quad (16)$$

Equation (15) is a basic two-parameter Weibull distribution with the scale parameter  $\sigma_{\text{ref}}$  and shape parameter  $\beta(\rho + 1)$ , termed  $\alpha$ , which is how an

experimentalist would be most likely to parameterize the strength distribution. However, Eq. (16) is necessary to provide consistency in the modeling framework by recasting the dependent parameter  $t_{\text{ref}}$  in terms of  $\sigma_{\text{ref}}$ ,  $R$  and  $\rho$ .

In the case of stress rupture lifetime testing, the cumulative distribution function for time to failure simplifies from (12) to:

$$\begin{aligned} F_{\text{CPL-W},\bar{\sigma}}(t) &= 1 - \exp \left\{ - \left[ \left( \frac{\bar{\sigma}}{\sigma_{\text{ref}}} \right)^\rho \frac{t}{t_{\text{ref}}} \right]^\beta \right\} \\ &= 1 - \exp \left\{ - \left[ \left( \frac{\bar{\sigma}}{\sigma_{\text{ref}}} \right)^\rho \frac{R(\rho + 1)t}{\sigma_{\text{ref}}} \right]^\beta \right\} \end{aligned} \quad (17)$$

Thus the CPL-W model can be given in general by (12), with a strength distribution given by (14) and a lifetime distribution given by (17). This model has three parameters:  $\sigma_{\text{ref}}$ ,  $\rho$ , and  $\beta$ . The CPL-W model can be obtained from (6) by taking the limit as  $r \rightarrow \infty$  and assuming  $\sigma(t) < \sigma_{\text{ref}}$ .

Regarding the role of loading rate, if we change the loading rate such that now  $s = R't$ , (14) becomes

$$\begin{aligned} F_{\text{CPL-W},s}(s) &= 1 - \exp \left\{ - \left[ \left( \frac{s}{\sigma_{\text{ref}}} \right)^\rho \frac{s}{R' t_{\text{ref}} (\rho + 1)} \right]^\beta \right\} \\ &= 1 - \exp \left\{ - \left[ \left( \frac{s}{\sigma_{\text{ref}}} \right)^\rho \frac{R s}{R R' t_{\text{ref}} (\rho + 1)} \right]^\beta \right\} \end{aligned} \quad (18)$$

and using (16),  $\sigma_{\text{ref}} = R t_{\text{ref}} (\rho + 1)$ , then (18) becomes

$$F_{\text{CPL-W},s}(s) = 1 - \exp \left\{ - \left[ \frac{s}{\sigma_{\text{ref}}} \left( \frac{R'}{R} \right)^{1/(\rho+1)} \right]^{(\rho+1)\beta} \right\} \quad (19)$$

In this case, we can define

$$\sigma'_{\text{ref}} = \sigma_{\text{ref}} \left( \frac{R'}{R} \right)^{1/(\rho+1)} \quad (20)$$

which relates the scale parameter at one loading rate to that for another loading rate.

To establish the reference strength,  $\sigma_{\text{ref}}$ , for resin impregnated strands or tows, the loading rate is chosen to generate tensile failure in say 10–30 s. All of the lifetime data, at different stress levels, are with respect to that reference strength value. Where caution is necessary is when data for one composite structure are generated at a loading rate that is different from another composite structure of the same

materials. For instance, in larger composite structures like COPV’s pressurization in a burst can take 10–30 min, or even longer. Thus, the loading rate for two composite structures of the same material but different sizes may differ by up to two orders of magnitude. Consequently, a stress ratio of, say,  $\sigma/\sigma_{ref} = 0.75$  in the two cases will produce very different lifetimes. Thus, loading rate is not a parameter to be fitted, but is an inputted parameter, chosen carefully to establish a reference strength, and in the discussion of the models we have kept the loading rate effectively fixed.

The fibers used in composite structures and the composites themselves do exhibit strengths that increase with loading rate over practical rates. In some cases, such as with Kevlar, the strength does tend to level off at very high loading rates, most likely due to a molecular mechanism change. However, the same is not seen in other polymer fibers, such as Zylon or Vectran, at similar loading rates, nor in S-glass fibers. Thus, the leveling off effect, if it exists, is not really a useful concept in stress rupture.

### Crack-growth model

The crack-growth model was also developed in the 1980s for a single fiber and has seen relatively little use. It is based on the mechanics of a crack propagating through a single fiber following the Paris crack-growth law, and assumes an initial distribution for the length of the largest crack and a fixed critical stress intensity factor, all chosen to result in a Weibull strength distribution. While originally derived in [9], an alternate derivation is provided in Appendix of [30]. The crack-growth model has been applied as a model for general composite failure, though without micromechanical justification in terms of cracks physically growing through the overall composite. This model is a special case of (6) as it can be obtained by setting  $r = \rho - 2$ :

$$F_{crack}(t|\sigma) = 1 - \exp \left\{ - \sup_{0 \leq \tau \leq t} \left[ \left( \frac{\sigma(\tau)}{\sigma_{ref}} \right)^{\rho-2} + \int_0^\tau \left( \frac{\sigma(s)}{\sigma_{ref}} \right)^\rho \frac{ds}{t_{ref}} \right]^\beta \right\} \tag{21}$$

where all the variables have the same meanings as before.

In the case of strength testing, the cumulative distribution function for failure stress is:

$$F_{crack,s}(s) = 1 - \exp \left\{ - \left[ \left( \frac{s}{\sigma_{ref}} \right)^{\rho-2} + \left( \frac{s}{\sigma_{ref}} \right)^\rho \frac{s}{Rt_{ref}(\rho+1)} \right]^\beta \right\} \\ = 1 - \exp \left\{ - \left[ \left( \frac{s}{\sigma_{ref}} \right)^\rho \left( \left( \frac{s}{\sigma_{ref}} \right)^{-2} + \frac{s}{Rt_{ref}(\rho+1)} \right) \right]^\beta \right\} \tag{22}$$

where again the stress level at failure is  $s = Rt$ .

If the constraint (18), only required for the CPL-W model, is applied to (22), the resulting strength distribution is:

$$F_{crack,s}(s) = 1 - \exp \left\{ - \left[ \left( \frac{s}{\sigma_{ref}} \right)^{\rho-2} \left( 1 + \left( \frac{s}{\sigma_{ref}} \right)^3 \right) \right]^\beta \right\}. \tag{23}$$

In the case of stress rupture lifetime testing, and ignoring the constraint (18), the cumulative distribution function for time to failure simplifies from (21) to:

$$F_{crack,\sigma}(t) = 1 - \exp \left\{ - \left[ \left( \frac{\bar{\sigma}}{\sigma_{ref}} \right)^{\rho-2} + \left( \frac{\bar{\sigma}}{\sigma_{ref}} \right)^\rho \frac{t}{t_{ref}} \right]^\beta \right\} \\ = 1 - \exp \left\{ - \left[ \left( \frac{\bar{\sigma}}{\sigma_{ref}} \right)^\rho \left( \left( \frac{\bar{\sigma}}{\sigma_{ref}} \right)^{-2} + \frac{t}{t_{ref}} \right) \right]^\beta \right\} \tag{24}$$

In general, the strength decay model is given by (21), with a strength distribution given by (22) and a lifetime distribution given by (24). Thus, in general this model has four parameters:  $\sigma_{ref}$ ,  $\rho$ ,  $\beta$ , and  $t_{ref}$ .

### Strength decay model

The most recently proposed model for stress rupture is the strength decay model [11, 31]. This model is purely a phenomenological model. There has been no statistical analysis to show whether it fits experimental data any better or worse than CPL-W. The strength decay model is also of the form (6) (as shown in Appendix of [30]), which is for a single fiber, and as with the previous models there is no compelling rationale as to why it should be applicable to a general composite structure. The strength decay model is obtained from (6) by setting  $r = \rho$ :

$$F_{\text{decay}}(t|\sigma) = 1 - \exp\left\{-\sup_{0 \leq \tau \leq t} \left\{ \left[ \left( \frac{\sigma(\tau)}{\sigma_{\text{ref}}} \right)^\rho + \int_0^\tau \left( \frac{\sigma(s)}{\sigma_{\text{ref}}} \right)^\rho \frac{ds}{t_{\text{ref}}} \right]^\beta \right\}\right\} \quad (25)$$

where all the variables have the same meanings as before.

In the case of strength testing, the cumulative distribution function for failure stress is:

$$F_{\text{decay},s}(s) = 1 - \exp\left\{-\left[\left(\frac{s}{\sigma_{\text{ref}}}\right)^\rho \left(1 + \frac{s}{Rt_{\text{ref}}(\rho+1)}\right)\right]^\beta\right\}. \quad (26)$$

where again  $s = Rt$  is the stress level at failure.

If the constraint (18), only required for the CPL-W model, is applied to (26), the resulting three-parameter strength distribution is:

$$F_{\text{decay},s}(s) = 1 - \exp\left\{-\left[\left(\frac{s}{\sigma_{\text{ref}}}\right)^\rho \left(1 + \frac{s}{\sigma_{\text{ref}}}\right)\right]^\beta\right\}. \quad (27)$$

In the case of stress rupture lifetime testing, and ignoring the constraint (18), the cumulative distribution function for time to failure simplifies from (25) to:

$$F_{\text{decay},\bar{\sigma}}(t) = 1 - \exp\left\{-\left[\left(\frac{\bar{\sigma}}{\sigma_{\text{ref}}}\right)^\rho \left(1 + \frac{t}{t_{\text{ref}}}\right)\right]^\beta\right\}. \quad (28)$$

In general, the strength decay model is given by (25), with a strength distribution given by (26) and a lifetime distribution given by (28). Thus, in general this model has four parameters:  $\sigma_{\text{ref}}$ ,  $\rho$ ,  $\beta$ , and  $t_{\text{ref}}$ .

Note that the constraint, (18), applied in (23) and (27), naturally arose in the special case of the CPL-W model and is not required by the 1979 functional form in general or any instances of it. Applying the constraint, however, does reduce by one the number of independent parameters to be estimated. In some circumstances, particularly when data are sparse, this may help in estimating failure probabilities.

## Comparing basic model behavior

The current state of probabilistic models, particularly those of the type considered here, is that there are three vying models, plus the overall functional form. These models all give either exactly or approximately

a Weibull distributed strength distribution as well as Weibull distributed lifetime distributions. This is key as actual experimental data for strength and life are typically Weibull distributed [15, 17].

As discussed in the introduction, some strength datasets and some lifetime datasets do have non-Weibull features, but most are well described by a standard two-parameter Weibull. According to [17], a lower tail that curves downwards from the straight Weibull prediction is frequently the result of truncating, in which weak specimens are not reported for a variety of reasons. One reason is that there can be a selection bias such that only strong(er) specimens are tested. Sometimes there is a kink in the strength distribution, such as in [17]. This kink may be caused by a truncation in the strength distribution at higher stress levels and/or faster loading rates, due to a change in the molecular mechanism. In lifetime distributions, occasionally there is a compressed upper tail, which has been known to happen when specimens originate from two sources and the weak ones fail early and dominate the short term portion of the distribution, while the stronger ones dominate the long-term tail of the lifetime distribution [17].

As it turns out, the main point of difference in the models compared is how the strength distribution relates to the lifetime distribution as is explored below.

## Comparing lifetime distributions

The lifetime distributions for the 1979 functional form, the CPL-W model, the crack-growth model and the strength decay model are given by (10), (17), (24) and (28), respectively, and can be framed as:

$$F_{\bar{\sigma}}(t) = 1 - \exp\left\{-\left[\left(\frac{\bar{\sigma}}{\sigma_{\text{ref}}}\right)^\rho \left(\Phi + \frac{t}{t_{\text{ref}}}\right)\right]^\beta\right\} \quad (29)$$

where

$$\Phi(\bar{\sigma}) = \begin{cases} (\bar{\sigma}/\sigma_{\text{ref}})^{r-\rho}, & \text{1979 functional form} \\ 0, & \text{CPL - W model} \\ (\bar{\sigma}/\sigma_{\text{ref}})^{-2}, & \text{crack - growth model} \\ 1, & \text{strength decay model} \end{cases} \quad (30)$$

In applications for moderate  $\bar{\sigma}/\sigma_{\text{ref}}$ , the factor  $\Phi + t/t_{\text{ref}}$  is dominated by the ratio  $t/t_{\text{ref}}$  at all but the shortest times. If the stress ratio,  $\bar{\sigma}/\sigma_{\text{ref}}$ , is small (say less than 0.3), and if the exponent arising in two of the versions of  $\Phi$ , namely  $r - \rho$  and  $-2$ , is negative, and when  $t_{\text{ref}}$  happens to be large, then it may take some



time before the  $t/t_{ref}$  term dominates, though in the meantime no failures will happen at such low stress ratios. Because  $t/t_{ref}$  is generally significantly greater than  $\Phi$  when the failure probability is significant, the lifetime distributions are effectively the same for these four models. Testing strategies for distinguishing among the models will not be discussed here, but nonetheless distinguishing features among the various models are presented below.

To simplify the notation when exploring the behavior of Eq. (29), the stress ratio  $\bar{\sigma}/\sigma_{ref}$  is called SR, such that  $\Phi = SR^\varpi$ , where  $\varpi$  is an exponent ranging across the real number line, but typically  $\varpi \geq -2$ . In practice, the stress ratio ranges from zero to one. For all positive values of  $\varpi$ ,  $\Phi$  is less than or equal one. Even for negative values, such as  $\varpi = -2$  as in the crack-growth model, the term  $\Phi = SR^\varpi$  remains under 10 for  $SR \geq 0.32$ , meaning that the normalized time  $T = t/t_{ref}$  will start to dominate  $\Phi$  once  $t \geq 10 t_{ref}$ . On the other hand, if when  $SR < 0.32$  and  $\varpi \leq -2$ , thus causing larger values of  $\Phi$ ,  $t$  must be much larger than  $t_{ref}$  for  $T$  to dominate  $\Phi$ . The key observation, once again, is that with such a low load level there are unlikely to be early failures observed experimentally. Thus, experimentally observable differences between the models are very unlikely to occur.

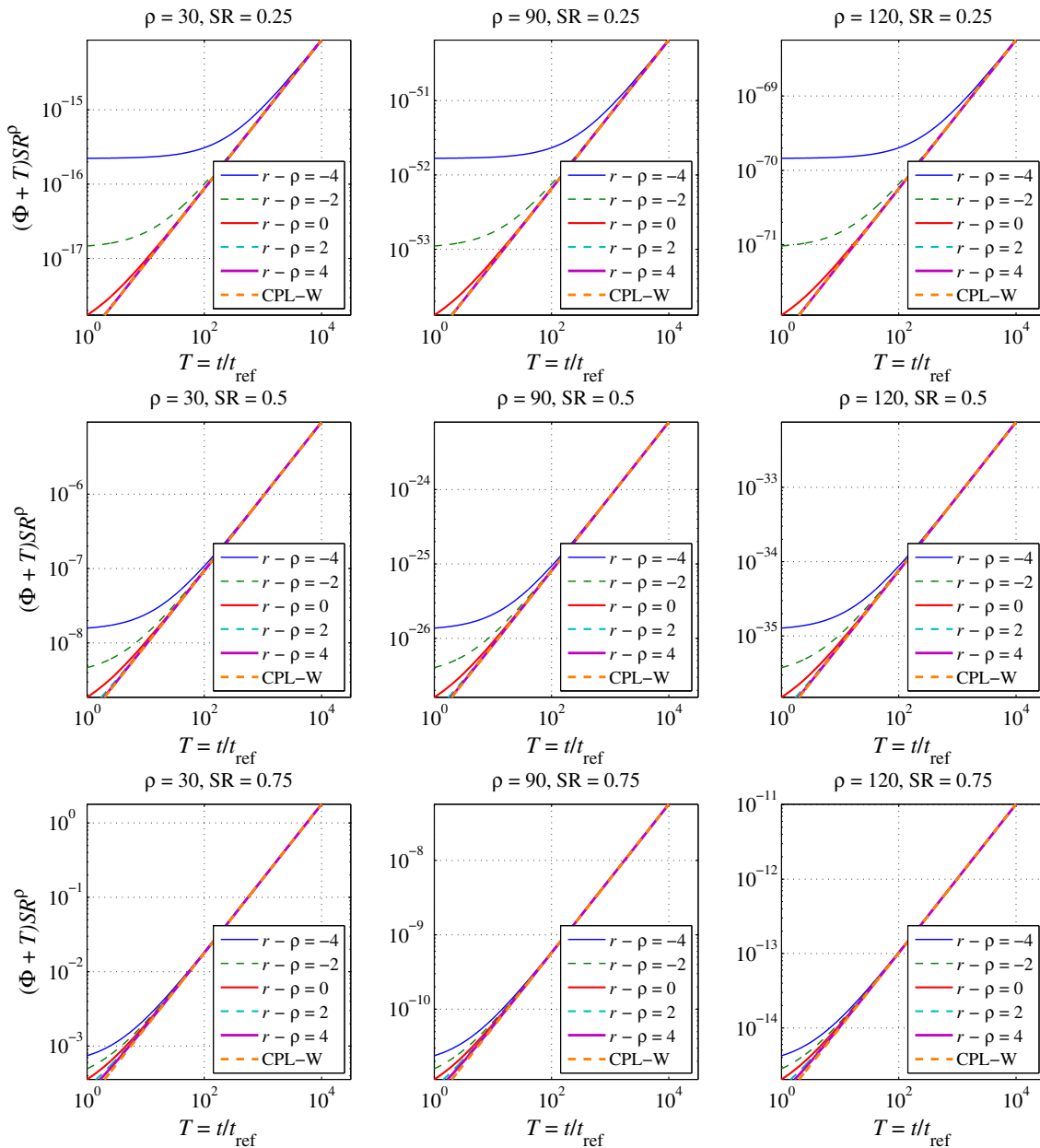
A comparison of the numerical values for  $\Phi = SR^\varpi$  and  $T = t/t_{ref}$  shows that in most cases  $SR^\varpi$  is dominated by  $T$ , and thus the lifetime distributions are effectively the same. This comparison is done in Fig. 1, which plots the key part of (29),  $(\Phi + T)SR^\rho$ , for scaled time  $T = t/t_{ref}$ . This interior part is plotted instead of plotting the full CDF so as to avoid a specific choice of  $\beta$ . In the case where  $\beta = 1$ , a plot of the cumulative distribution function (CDF) of the failure probability is approximately the same figure, since  $10^{-n} \approx 1 - \exp\{-10^{-n}\}$ ,  $n \geq 2$ . Thus, for Fig. 1 the top two rows of plots can be viewed as failure probabilities with  $\beta = 1$ . In cases where  $\beta \neq 1$ , then the axis label is related to the failure probability by  $10^{-\beta n} \approx 1 - \exp\{-10^{-\beta n}\}$ ,  $n \geq 2$ , such that the failure probability can be calculated by multiplying the exponent by  $\beta$  in each axis label. For instance, in the uppermost left panel of Fig. 1, if  $\beta = 1/3$ , then  $10^{-15}$  becomes  $10^{-5}$ ,  $10^{-16}$  becomes  $10^{-5.33}$ , and  $10^{-17}$  becomes  $10^{-5.66}$ , and these values are then seen as failure probabilities.

Figure 1 shows that, in all plotted cases, the models converge by the time  $T = 10^4$ . This convergence happens sooner for larger stress ratios (at the bottom of the figure), yet as the stress ratio increases the numerical value of  $(\Phi + T)SR^\rho$  increases. Thus, assuming  $\beta$  is held constant, it is more likely for failures to occur at lower times with higher stress ratios. This is also true as  $\rho$  decreases, since smaller values of  $\rho$  result in larger values of  $(\Phi + T)SR^\rho$ .

In carbon fiber composites, where the design stress ratio is typically 0.5,  $t_{ref}$  is typically less than one, generally between  $10^{-2}$  and  $10^{-5}$ . In these cases, the models mostly converge by the time  $T = 10^2$ , corresponding to times between  $10^{-3}$  and 1 h. Thus, for carbon, under a stress ratio of interest, the models predict the same life behavior for lifetimes of interest, unless  $\beta$  is particularly low. A  $(\Phi + T)SR^\rho$  value of  $10^{-7}$ , when  $\beta = 1$  corresponds to a failure probability of  $10^{-7}$ , i.e., almost certain survival. For carbon fiber composites however,  $\beta$  is typically less than 0.3, and for T1000 carbon/epoxy tows can be as low as 0.07, though coupled with a much larger value of  $\rho$ , corresponding to the right column in Fig. 1. Assuming  $\rho$  is fixed and small, for low  $\beta$  values the failure probability is higher, e.g.,  $\approx 0.01$  when  $\beta = 0.3$  and  $(\Phi + T)SR^\rho = 10^{-7}$ , and likely unacceptable from a design point of view. However, to obtain  $(\Phi + T)SR^\rho = 10^{-7}$  the stress ratio has to be high and the value of  $\rho$  has to be low, i.e., corresponding to the bottom of the left-hand column in Fig. 1. From the point of view of running experiments, however, the models will remain indistinguishable because the probability of getting failures in such short times is so small, even in a relatively large sample.

For Kevlar, there is more difference, as  $t_{ref}$  for Kevlar may be between 1 and 10 h, and the stress ratio may be lower; however, conversely  $\beta$  for Kevlar is typically greater than 1. Even for a stress ratio of 0.25 though, all models for which  $r - \rho \geq -2$  agree fairly well after  $T = 100$ , and fully by  $T = 1000$ , where for Kevlar  $T = 1000$  corresponds to times between 1000 and 10000 h.

In [11], the lifetime distribution of the strength decay and CPL-W models are compared, with the results being identical after the first half hour in the case of an IM6 carbon fiber/epoxy composite system. Some model differences are reported when the parameters for each model are calculated



**Figure 1** Plot of  $(\Phi + T)SR^\rho$ , where  $T = t/t_{ref}$  and  $SR = \bar{\sigma}/\sigma_{ref}$ , for values of  $r$  including  $r = \rho - 2$ , the crack-growth model, and  $r = \rho$ , the strength decay model. The term  $SR^\rho T$  is also plotted, to correspond with the CPL-W model, wherein  $\Phi \equiv 0$ .

independently; however, this could be attributed to estimation error for the parameters.

**Comparing strength distributions**

The strength distributions for the 1979 functional form, the CPL-W model, the crack-growth model and the strength decay model are given by (8), (14), (22) and (26), respectively, and can be framed as:

$$F_s(s) = 1 - \exp\left\{-\left[\left(\frac{s}{\sigma_{ref}}\right)^\rho \left(\Phi + \frac{s}{Rt_{ref}(\rho + 1)}\right)\right]^\beta\right\} \tag{31}$$

where the term  $\Phi$ , defined in (30), is here a function of  $s$ .

One simplification is to assume the constraint on  $t_{ref}$  as given in (18), namely  $\sigma_{ref} = Rt_{ref}(\rho + 1)$ , which eliminates  $t_{ref}$  as an independent parameter. However, the artificiality of this is that the effect of

increasing the loading rate is to change the other parameter values. Equation (31) simplifies to:

$$F_s(s) = 1 - \exp\left\{-\left[\left(\frac{s}{\sigma_{ref}}\right)^\rho \left(\Phi + \frac{s}{\sigma_{ref}}\right)\right]^\beta\right\}. \quad (32)$$

However, strictly speaking, the constraint is not a consequence of the structure of the 1979 functional form and only naturally arises in the CPL-W model.

To help visualize (32), with the constraint, Fig. 2 plots the interior quantity

$$\left(\frac{s}{\sigma_{ref}}\right)^\rho \left(\Phi + \frac{s}{\sigma_{ref}}\right), \quad (33)$$

as a function of the stress ratio,  $s/\sigma_{ref}$ , for several values of  $\rho$ . As before, the interior part is plotted instead of plotting the entirety of Eq. (33) so as to avoid a specific choice of  $\beta$ . To remind the reader, the axis label is related to the failure probability for a given value of  $\beta$ , via  $10^{-\beta n} \approx 1 - \exp\{-10^{-\beta n}\}$ ,  $n \geq 2$ , such that the failure probability can be calculated by multiplying the exponent by  $\beta$  in each axis label. For an example, see the discussion of Fig. 1.

From Fig. 2, it is clear that the quantity in Eq. (33) varies considerably across the different models, particularly for low  $\rho$  values. Also, for all models except the CPL-W model, the lines are not straight but rather have a kink around a stress ratio of one, which is typically a bit higher than the mean strength.

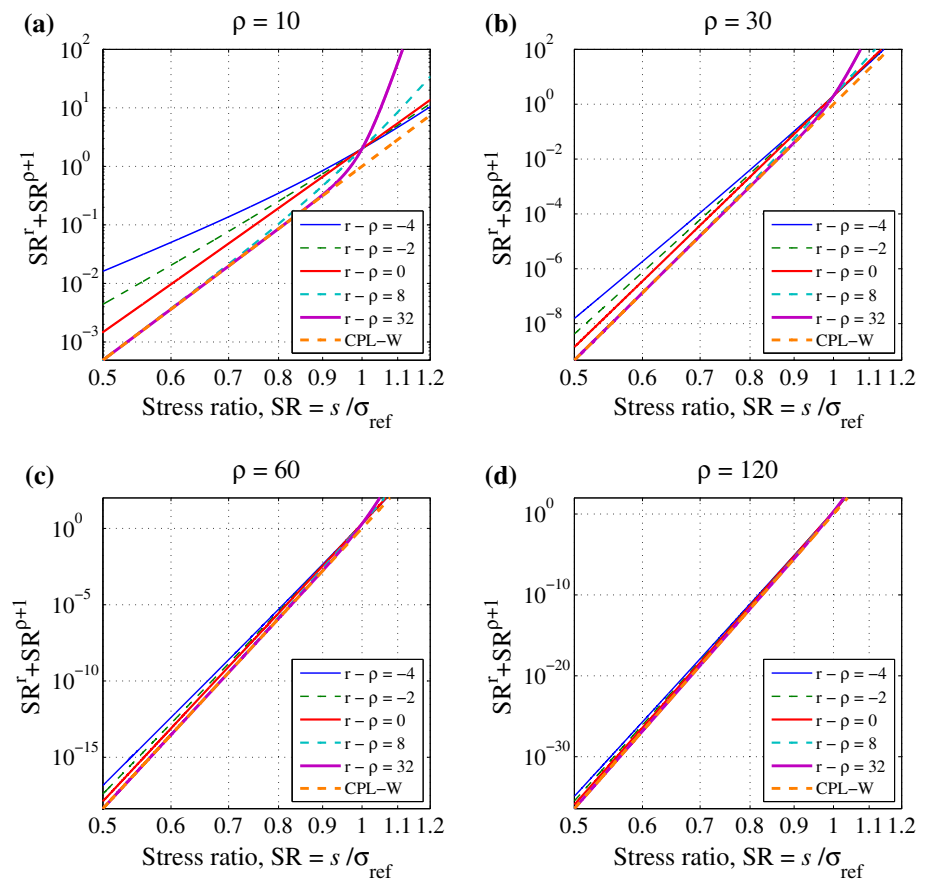
The CPL-W model provides a lower bound to the various instances of the 1979 functional form. For stress ratios less than 1, instances of the 1979 functional form where  $r - \rho$  is more negative correspond to the uppermost lines, and all models for which  $r - \rho > 0$  are approximately equal to the CPL-W model. In contrast, for stress ratios above 1, instances of the 1979 functional form where  $r - \rho$  is larger correspond to the uppermost lines.

The constraint (18) is applied in Fig. 2 and Eqs. (32) and (33). If that constraint is removed, however, (31) can be restored to

$$F_s(s) = 1 - \exp\left\{-\left\{\left[\left(\frac{s}{\sigma_{ref}}\right)^\rho \left(\Phi + \frac{s}{\sigma_{ref}K}\right)\right]^\beta\right\}\right\} \quad (34)$$

where

**Figure 2** Plot of (33) for  $\rho$  values of **a** 10, **b** 30, **c** 60 and **d** 120, comparing the CPL-W model against various instances of the 1979 functional form, including the crack-growth model ( $r - \rho = -2$ ) and the strength decay model ( $r = \rho$ ).



$$K = \frac{Rt_{ref}(\rho + 1)}{\sigma_{ref}} \tag{35}$$

is now allowed to vary, including in the CPL-W model. Now, the key interior part becomes

$$\left(\frac{s}{\sigma_{ref}}\right)^\rho \left(\Phi + \frac{s}{\sigma_{ref}K}\right). \tag{36}$$

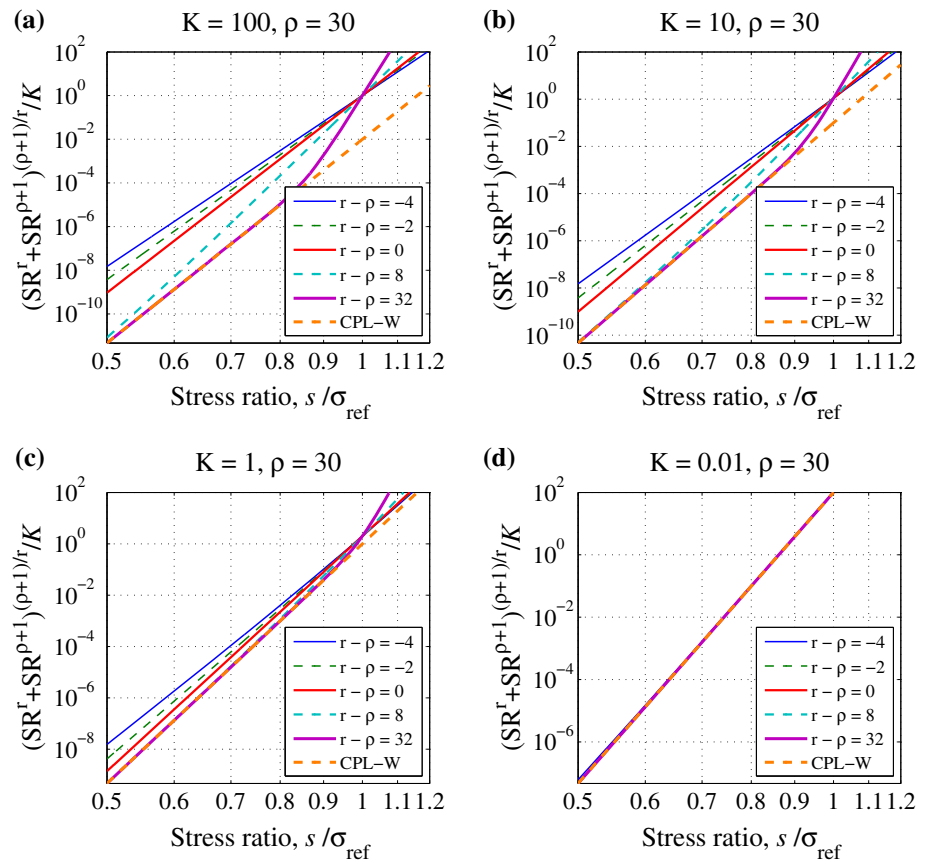
Note that  $K$  is proportional to the loading rate,  $R$ . Experimentally, the strength distribution is known to depend on the loading rate, with faster loading generally resulting in a higher experimental value for  $\sigma_{ref}$ .

Figure 3 plots (36) for various values of  $K$ , showing that by allowing  $K$  to vary the models become more different when  $K > 1$  and more similar when  $K \leq 1$ . As before, the CPL-W model provides a lower bound on models from the 1979 functional form. It is interesting to note that all the models collapse to the same line for small  $K$ . The largest difference between the models corresponds to large values of  $K$ , i.e., fast loading rates.

For all values of  $K$ , the CPL-W model retains the same slope and simply shifts down as  $K$  increases. The same is not true for the instances of the 1979 functional form, because while they do shift as  $K$  increases, the slope of their central straight regions varies as well. The slope has the most variation for large values of  $K$ , but once  $K < 1$  the slope has converged, for all instances of the 1979 functional form, to the CPL-W model’s slope. If varying  $K$  is viewed as varying the loading rate, this implies that for the CPL-W model changing the loading rate results purely in a different value of the scale parameter. In contrast, for the 1979 models, a change in loading rate can result in both a change of the scale parameter and the shape parameter. These are general observations from Fig. 3.

Focusing on the cases  $K = 10$  and  $K = 100$ , in the upper straight regions where test data are most likely to occur, a scaling can be chosen to collapse the various instances of the 1979 functional form onto one common line, which happens to be the line for the CPL-W model. If we consider modifying (36) to

**Figure 3** Plot of (36) for  $K$  values of **a** 100, **b** 10, **c** 1, and **d** 0.1, comparing the CPL-W model against various instances of the 1979 functional form, including the crack-growth model ( $r - \rho = -2$ ) and the strength decay model ( $r = \rho$ ), where  $\rho = 30$ .



$$\frac{1}{K} \left[ \left( \frac{s}{\sigma_{\text{ref}}} \right)^\rho \left( \Phi + \frac{s}{\sigma_{\text{ref}} K} \right) \right]^{\frac{\rho+1}{r}}, \tag{37}$$

which amounts to a subtle redefinition of several of the parameters, then the lines collapse to the CPL-W model (without the constraint), as desired above, at least for values of (37) where data are likely to be easily collected. This is shown in Fig. 4a.

The rationale for (37) is that for  $K > 1$  the term  $s/(\sigma_{\text{ref}}K)$  becomes small as compared to  $\Phi$ . Thus, (37) can be approximated by:

$$\begin{aligned} & \frac{1}{K} \left[ \left( \frac{s}{\sigma_{\text{ref}}} \right)^\rho \left( \Phi + \frac{s}{\sigma_{\text{ref}} K} \right) \right]^{\frac{\rho+1}{r}} \\ & \approx \frac{1}{K} \left[ \left( \frac{s}{\sigma_{\text{ref}}} \right)^\rho \Phi \right]^{\frac{\rho+1}{r}} \left[ 1 + \frac{1}{r} \left( \frac{s}{\Phi R t_{\text{ref}}} \right) \right]. \end{aligned} \tag{38}$$

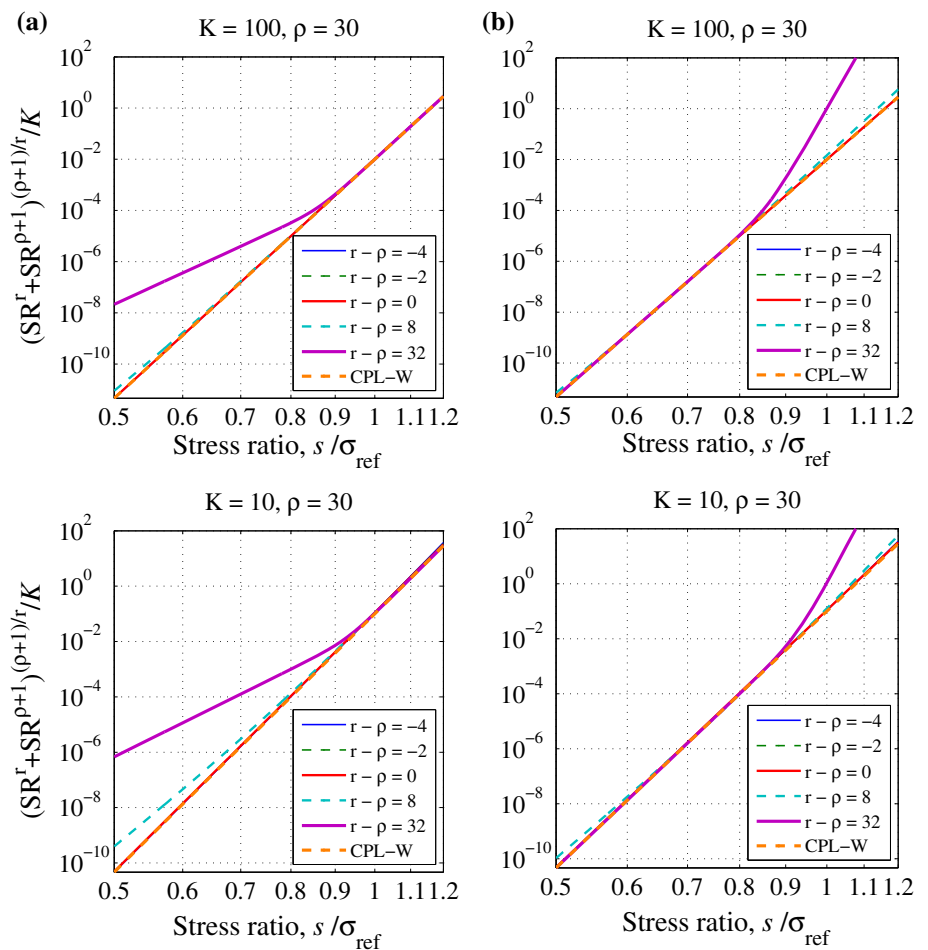
Recalling in the 1979 model that according to (30)  $\Phi = (s/\sigma_{\text{ref}})^{r-\rho}$ , and by (35)  $K = R t_{\text{ref}}(\rho + 1)/\sigma_{\text{ref}}$ , (38) becomes

$$\begin{aligned} & \frac{1}{K} \left[ \left( \frac{s}{\sigma_{\text{ref}}} \right)^\rho \Phi \right]^{\frac{\rho+1}{r}} \left[ 1 + \frac{s}{\Phi r R t_{\text{ref}}} \right] \\ & = \frac{\sigma_{\text{ref}}}{R t_{\text{ref}}(\rho + 1)} \left( \frac{s}{\sigma_{\text{ref}}} \right)^{\rho+1} \left[ 1 + \left( \frac{s}{\sigma_{\text{ref}}} \right)^{\rho+1-r} \frac{\sigma_{\text{ref}}}{r R t_{\text{ref}}} \right] \\ & \approx \frac{\sigma_{\text{ref}}}{R t_{\text{ref}}(\rho + 1)} \left( \frac{s}{\sigma_{\text{ref}}} \right)^{\rho+1}. \end{aligned} \tag{39}$$

which is the CPL-W model’s interior term. This approximation works well so long as  $r - \rho < 30$ , as can be seen in Fig. 4a. Whether or not  $r - \rho < 30$  corresponds to a physical material is unknown.

A different scaling can be done to instead scale the lower straight regions in Fig. 3, as can be

**Figure 4** Plot of (37) for  $K$  values of 100, and 10, comparing the CPL-W model against various instances of the 1979 functional form, including the crack-growth model ( $r - \rho = -2$ ) and the strength decay model ( $r = \rho$ ), where  $\rho = 30$ . In **a**, the upper portions are collapsed, whereas in **b** the lower portions are collapsed.



seen in Fig. 4b. This scaling was done by trial and error.

The implication of Fig. 4 for  $K > 1$ , along with Fig. 3 for  $K < 1$ , is that all of the models can still be said to have Weibull distributed strength as far as is likely to be discriminated from even a large practical dataset.

If one fits a Weibull distribution to experimental data, the Weibull shape and scale parameter values estimated are the same irrespective of any model subtleties. How the values of these estimated parameters will relate to the various model parameters  $\sigma_{\text{ref}}$ ,  $r$ ,  $\rho$ ,  $\beta$ , and  $t_{\text{ref}}$ , will differ among the models. In particular, for the CPL-W model  $\sigma_{\text{ref}}$  is the inherent Weibull scale parameter, yet for the 1979 functional form  $\sigma_{\text{ref}}$  varies as a function of  $K$ .

## Proof testing

In applications, all COPVs typically undergo some form of proof testing (which may be combined with autofrettage), and thus model behavior under proof testing is of interest.

In idealized proof testing, the load profile is assumed to be:

$$\begin{aligned}\sigma(t) &= \sigma_p, \quad 0 \leq t < t_p \\ \sigma(t) &= \bar{\sigma}, \quad t_p \leq t\end{aligned}\quad (40)$$

where  $t_p > 0$  is the proof hold time,  $\sigma_p > 0$  is the proof load level, and  $\sigma_p > \bar{\sigma}$ . [In reality, there are ramp up and down times; however, these have a small effect compared to the proof hold time, largely because of the division by  $\rho + 1$ , as appears in the derivation of Eq. (8)].

The general cumulative distribution function for failure probability of the 1979 functional form is given in (6). In the case involving a proof test, substituting (40) into (6) gives the key quantity in the exponential as:

$$\begin{aligned}\sup_{0 \leq \tau \leq t} & \left[ \left( \frac{\sigma(t)}{\sigma_{\text{ref}}} \right)^r + \int_0^t \left( \frac{\sigma(\tau)}{\sigma_{\text{ref}}} \right)^\rho \frac{d\tau}{t_{\text{ref}}} \right]^\beta \\ &= \begin{cases} \left( \frac{\sigma_p}{\sigma_{\text{ref}}} \right)^r + \left( \frac{\sigma_p}{\sigma_{\text{ref}}} \right)^\rho \frac{t}{t_{\text{ref}}}, & 0 \leq t \leq t_p \\ \left( \frac{\sigma_p}{\sigma_{\text{ref}}} \right)^r + \left( \frac{\sigma_p}{\sigma_{\text{ref}}} \right)^\rho \frac{t_p}{t_{\text{ref}}}, & t_p \leq t \leq t_s, \\ \left( \frac{\bar{\sigma}}{\sigma_{\text{ref}}} \right)^r + \left( \frac{\sigma_p}{\sigma_{\text{ref}}} \right)^\rho \frac{t_p}{t_{\text{ref}}} + \left( \frac{\bar{\sigma}}{\sigma_{\text{ref}}} \right)^\rho \frac{t - t_p}{t_{\text{ref}}}, & t \geq t_s \end{cases}\end{aligned}\quad (41)$$

where  $t_s$  is called a ‘safe time’ as will be described below. The existence of this safe time leads to three distinct time regimes in (41), despite there being only two load levels. When the load drops from  $\sigma_p$  to  $\bar{\sigma}$  at time  $t_p$ , the first term on the left side in (41),  $(\sigma(t)/\sigma_{\text{ref}})^r$ , decreases in value, but the accumulated value of the left side cannot decrease since the cumulative probability of failure cannot decrease. This requirement is mathematically accounted for by using the ‘supremum’ operator, which essentially means the maximum value achieved up to the given time. It takes some additional time for the left-hand side to increase beyond the value it had at time  $t_p$ , i.e., the integral term must accumulate enough to compensate for the decrease in the first term due to the reduction of  $\sigma(t)$ . This amount of time can be found by equating the middle and last quantities in (41) and letting  $t = t_s$ , giving

$$\begin{aligned}\left( \frac{\sigma_p}{\sigma_{\text{ref}}} \right)^r + \left( \frac{\sigma_p}{\sigma_{\text{ref}}} \right)^\rho \frac{t_p}{t_{\text{ref}}} &= \left( \frac{\bar{\sigma}}{\sigma_{\text{ref}}} \right)^r + \left( \frac{\sigma_p}{\sigma_{\text{ref}}} \right)^\rho \frac{t_p}{t_{\text{ref}}} \\ &+ \left( \frac{\bar{\sigma}}{\sigma_{\text{ref}}} \right)^\rho \frac{t_s - t_p}{t_{\text{ref}}}.\end{aligned}\quad (42)$$

Solving for  $t_s$  yields

$$\begin{aligned}t_s &= t_{\text{ref}} \left( \frac{\bar{\sigma}}{\sigma_{\text{ref}}} \right)^{-\rho} \left[ \left( \frac{\sigma_p}{\sigma_{\text{ref}}} \right)^r - \left( \frac{\bar{\sigma}}{\sigma_{\text{ref}}} \right)^r \right] + t_p \\ &= t_{\text{ref}} \left( \frac{\bar{\sigma}}{\sigma_{\text{ref}}} \right)^{-\rho} \left[ \left( \frac{\sigma_p}{\bar{\sigma}} \right)^r - 1 \right] + t_p\end{aligned}\quad (43)$$

Thus, in the 1979 functional form the cumulative distribution function for time to failure, under the loading given by (40), is:

$$F_{1979p}(t) = \begin{cases} 1 - \exp\left\{-\left[\left(\frac{\sigma_p}{\sigma_{ref}}\right)^r + \left(\frac{\sigma_p}{\sigma_{ref}}\right)^\rho \frac{t}{t_{ref}}\right]^\beta\right\} & 0 < t \leq t_p \\ 1 - \exp\left\{-\left[\left(\frac{\sigma_p}{\sigma_{ref}}\right)^r + \left(\frac{\sigma_p}{\sigma_{ref}}\right)^\rho \frac{t_p}{t_{ref}}\right]^\beta\right\} & t_p < t \leq t_s \\ 1 - \exp\left\{-\left[\left(\frac{\bar{\sigma}}{\sigma_{ref}}\right)^r + \left(\frac{\sigma_p}{\sigma_{ref}}\right)^\rho \frac{t_p}{t_{ref}} + \left(\frac{\bar{\sigma}}{\sigma_{ref}}\right)^\rho \frac{t - t_p}{t_{ref}}\right]^\beta\right\} & t > t_s \end{cases} \tag{44}$$

where  $t_s$  is given in (43).

The time  $t_s$  is frequently termed the ‘safe time,’ as the cumulative failure probability does not increase for  $t_p < t \leq t_s$ , and thus the probability that a specimen that has survived to time  $t_p$  fails inside this range is zero, i.e., the specimens are safe from failures. The length of  $t_s - t_p$  increases as the ratio of proof load to sustained load,  $\sigma_p/\bar{\sigma}$ , increases, and as  $\rho$  increases, yet it decreases as  $r$  increases. The magnitude of this safe time can be extremely large in some cases. For instance, for  $\rho = 100$ , a proof ratio of  $\sigma_p/\bar{\sigma} = 1.5$ , a lifetime stress ratio of  $\bar{\sigma}/\sigma_{ref} = 0.5$ , and  $r - \rho \leq 40$ , then the scaled safe time,  $t_s/t_{ref}$ , is predicted to be at least 100,000. However, for  $\rho = 100$  and  $r - \rho \geq 60$  the scaled safe time becomes negligible.

In contrast to the general 1979 functional form and instances thereof, the CPL-W model [with or without the constraint on  $t_{ref}$  as given in (18)] has the cumulative distribution function for time to failure, with loading given by (40), of:

$$F_{CPL-Wp}(t) = \begin{cases} 1 - \exp\left\{-\left[\left(\frac{\sigma_p}{\sigma_{ref}}\right)^\rho \frac{t}{t_{ref}}\right]^\beta\right\}, & 0 < t \leq t_p \\ 1 - \exp\left\{-\left[\left(\frac{\sigma_p}{\sigma_{ref}}\right)^\rho \frac{t_p}{t_{ref}} + \left(\frac{\bar{\sigma}}{\sigma_{ref}}\right)^\rho \frac{t - t_p}{t_{ref}}\right]^\beta\right\}, & t > t_p \end{cases} \tag{45}$$

which has no safe time, but does have a decreased rate of failure for some time after the proof test. Note that for  $\sigma(t) < \sigma_{ref}$ , relevant to stress rupture, the CPL-W model can be obtained from the 1979 functional form by letting  $r - \rho \rightarrow \infty$ .

### Comparing model behavior in the case of proof testing

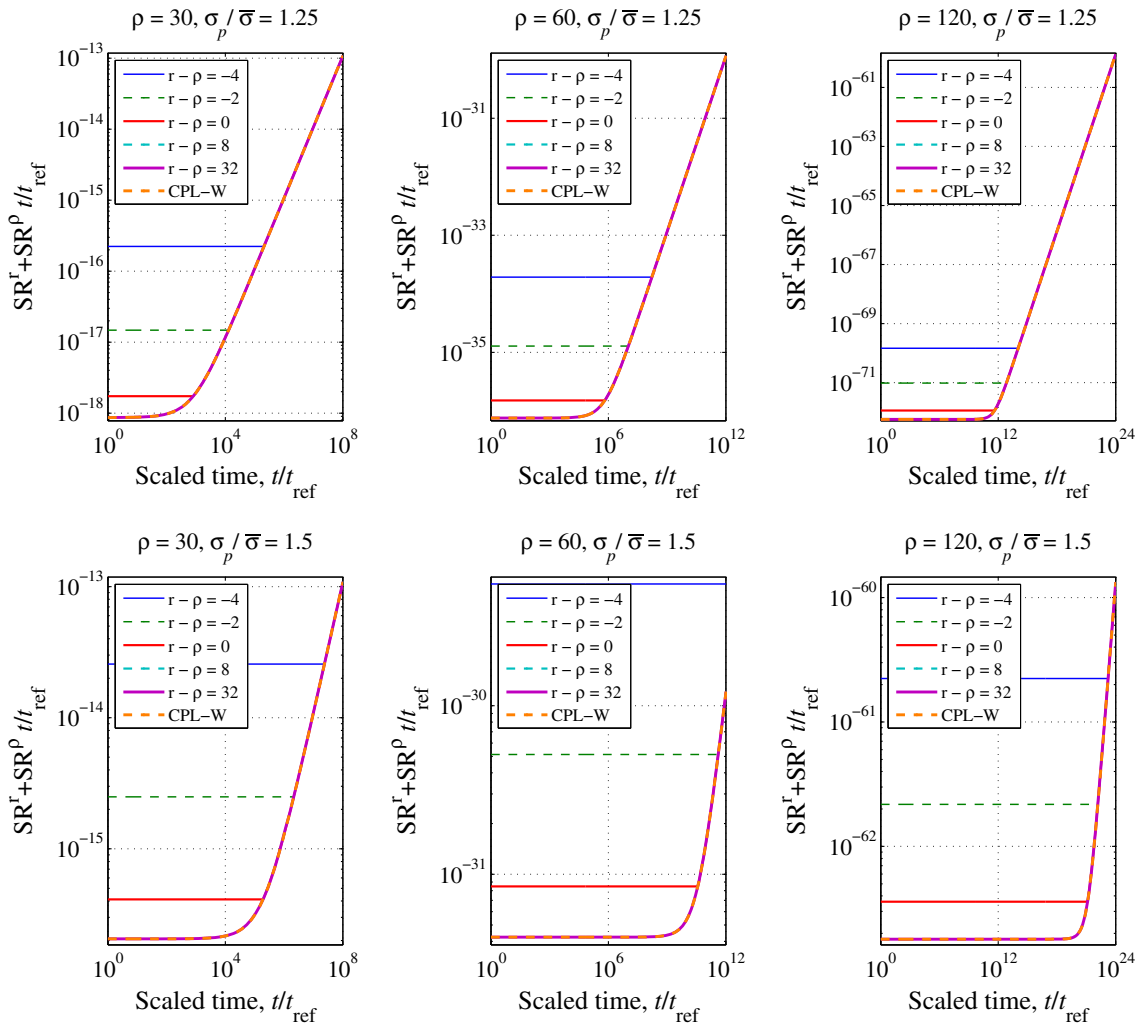
The biggest difference between the models, in the case of proof testing, is the behavior of the safe time  $t_s$ . Shortly after  $t_s$ , all instances of the 1979 functional form, created by varying the value of  $r - \rho$ , converge to the CPL-W model. Furthermore, the CPL-W model provides a lower bound on the cumulative failure probability, as can be seen in Fig. 5.

Figure 5 plots (41), the key interior part of (44), instead of plotting the entirety (44), so as to avoid a specific choice of  $\beta$ . Once again, the axis label is related to the failure probability for a given value of  $\beta$ , via  $10^{-\beta n} \approx 1 - \exp\{-10^{-\beta n}\}$ ,  $n \geq 2$ , such that the failure probability can be calculated by multiplying the exponent by  $\beta$  in each axis label. For an example, see the discussion of Fig. 1.

In Fig. 5, the 1979 functional form instances remain flat until  $T > T_s = t_s/t_{ref}$ , at which point they sharply increase, and quickly converge to the CPL-W model. As  $\rho$  increases, the value of  $T_s$  also increases. For instance, when  $\sigma_p/\bar{\sigma} = 1.5$  and  $\rho = 90$ , we find that  $T_s > 10^{10}$ , which corresponds to a time between  $10^5$  and  $10^{11}$  h, depending on the particular value of  $t_{ref}$ . The sensitivity of  $T_s$  to the parameters  $\sigma_p/\bar{\sigma}$ ,  $\rho$ , and  $r$  can be seen from Fig. 5. Intuitively, what Fig. 5 is illustrating is that once  $T_s$  is known, one can sketch the behavior of each of the models by first drawing the line for the CPL-W model, calculating  $T_s$ , and then drawing a horizontal line that intersects the CPL-W line at exactly  $T_s$ .

### Conditional reliability

The reliability,  $R(t)$ , for a specimen is defined as one minus the failure probability,  $F(t)$ , and conditional reliability following a proof test,  $R_p(t|\sigma_p)$ , is defined



**Figure 5** Plots of the key interior quantities in (44) and (45) for varying values of  $\rho$  and  $\sigma_p/\bar{\sigma}$ , where  $\bar{\sigma}/\sigma_{ref} = 0.5$  and  $T_p = t_p/t_{ref} = 1$ , for scaled time  $T = t/t_{ref}$ .

as the reliability given that this specimen has survived a proof test. This is, practically, a very useful concept as only COPVs that survive their proof tests can be used. Symbolically, the conditional probability can be calculated using Bayes theorem as:

$$R_p(t|\sigma_p) = \frac{R(t)}{R(t_p)} = \frac{1 - F(t)}{1 - F(t_p)} \tag{46}$$

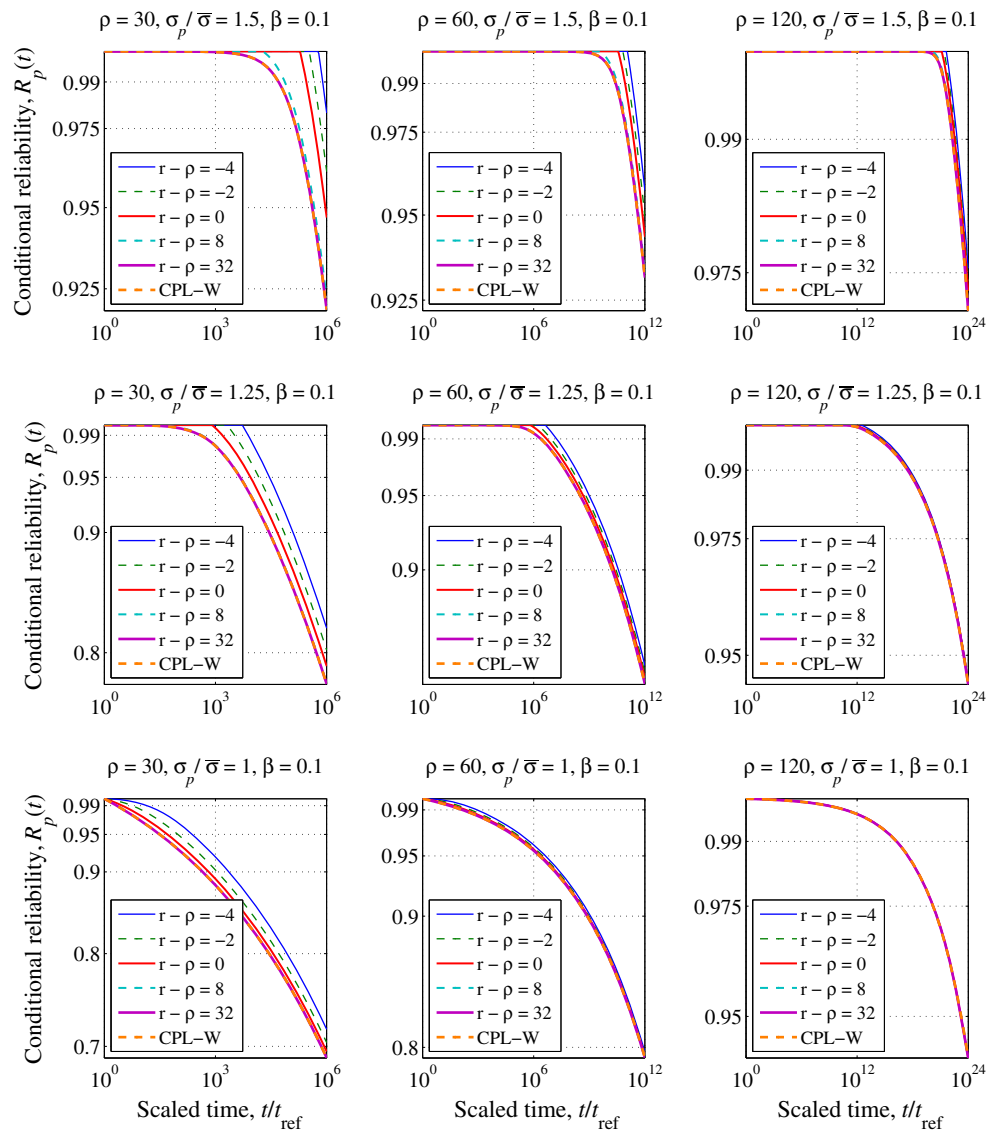
For the 1979 functional form, and thus the crack-growth and strength decay models, the reliability at  $t > t_p$  given survival of the proof test is:

$$R_{1979p}(t) = \begin{cases} 1, & t_p < t \leq t_s \\ \frac{\exp\left\{-\left[\left(\frac{\bar{\sigma}}{\sigma_{ref}}\right)^r + \left(\frac{\sigma_p}{\sigma_{ref}}\right)^\rho \frac{t_p}{t_{ref}} + \left(\frac{\bar{\sigma}}{\sigma_{ref}}\right)^\rho \frac{t - t_p}{t_{ref}}\right]^\beta\right\}}{\exp\left\{-\left[\left(\frac{\sigma_p}{\sigma_{ref}}\right)^r + \left(\frac{\sigma_p}{\sigma_{ref}}\right)^\rho \frac{t_p}{t_{ref}}\right]^\beta\right\}}, & t > t_s \end{cases} \tag{47}$$

or

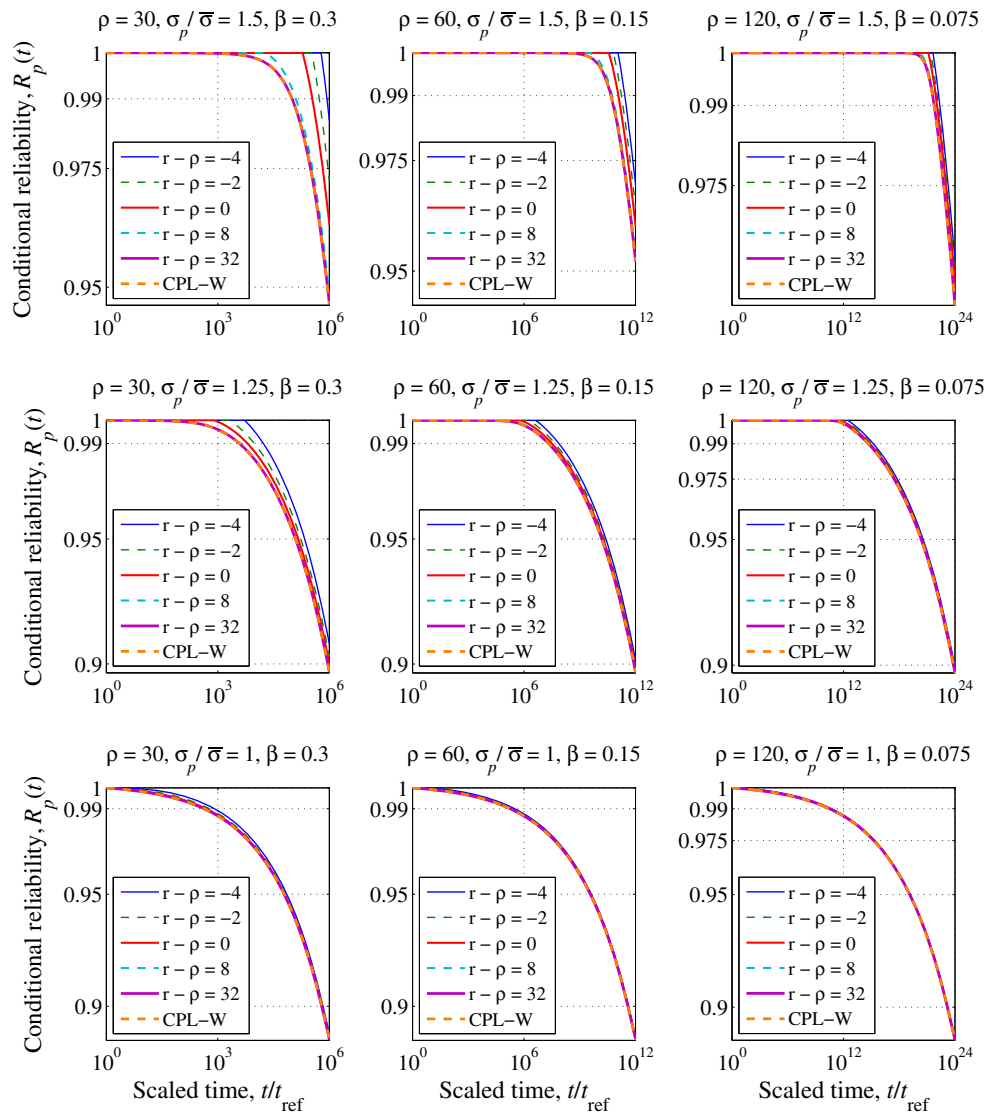


**Figure 6** Plot of conditional reliabilities (47) and (49) for varying values of  $\rho$  and  $\sigma_p/\bar{\sigma}$ , where  $\bar{\sigma}/\sigma_{ref} = 0.5$ ,  $T_p = t_p/t_{ref} = 1$ , and  $\beta = 0.1$ , for scaled time  $T = t/t_{ref}$ .



$$R_{1979p}(t) = \begin{cases} 1, & t_p < t \leq t_s \\ \exp \left\{ \left[ \left( \frac{\sigma_p}{\sigma_{ref}} \right)^r + \left( \frac{\sigma_p}{\sigma_{ref}} \right)^\rho \frac{t_p}{t_{ref}} \right]^\beta - \left[ \left( \frac{\bar{\sigma}}{\sigma_{ref}} \right)^r + \left( \frac{\sigma_p}{\sigma_{ref}} \right)^\rho \frac{t_p}{t_{ref}} + \left( \frac{\bar{\sigma}}{\sigma_{ref}} \right)^\rho \frac{t - t_p}{t_{ref}} \right]^\beta \right\}, & t < t_s \end{cases} \quad (48)$$

**Figure 7** Plot of conditional reliabilities (47) and (49) for varying values of  $\rho$ ,  $\beta$ , and  $\sigma_p/\bar{\sigma}$ , where  $\rho\beta = 9$ ,  $\bar{\sigma}/\sigma_{ref} = 0.5$ , and  $T_p = t_p/t_{ref} = 1$ , for scaled time  $T = t/t_{ref}$ .



For the CPL-W model, the conditional reliability for times,  $t$ , greater than  $t_p$  is given by:

loading is the same as the reliability conditional on the vessel surviving loading to the lifetime load. This

$$\begin{aligned}
 R_{CPL-W_p}(t) &= \exp \left\{ \left[ \left( \frac{\sigma_p}{\sigma_{ref}} \right)^\rho \frac{t_p}{t_{ref}} \right]^\beta - \left[ \left( \frac{\sigma_p}{\sigma_{ref}} \right)^\rho \frac{t_p}{t_{ref}} + \left( \frac{\bar{\sigma}}{\sigma_{ref}} \right)^\rho \frac{t - t_p}{t_{ref}} \right]^\beta \right\} \\
 &= \exp \left\{ \left[ \left( \frac{\sigma_p}{\sigma_{ref}} \right)^\rho \frac{t_p}{t_{ref}} \right]^\beta \left( 1 - \left[ 1 + \left( \frac{\bar{\sigma}}{\sigma_p} \right)^\rho \frac{t - t_p}{t_p} \right]^\beta \right) \right\}, \quad t > t_p
 \end{aligned}
 \tag{49}$$

Plots of these conditional reliabilities are given in Figs. 6 and 7, for values of  $\sigma_p/\bar{\sigma}$  of 1.5, 1.25 and 1. In the last case, a proof test equivalent to the lifetime

is the reliability of practical interest, as no vessel in service will be used if it does not survive its initial loading.

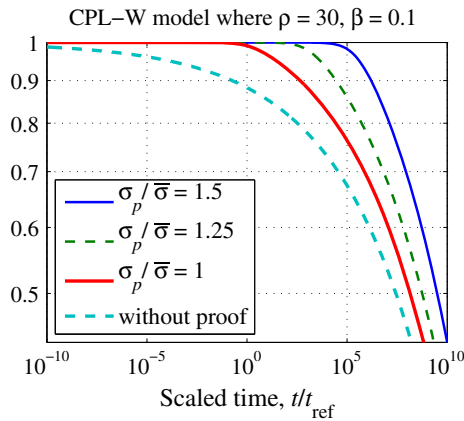


**Figure 8** Unconditional lifetime reliability and conditional reliabilities for the CPL-W model with  $\rho = 30$  and  $\beta = 0.1$ , for  $\sigma_p/\bar{\sigma}$  values of 1.5, 1.25 and 1, and where  $\bar{\sigma}/\sigma_{ref} = 0.5$ , and  $t_p/t_{ref} = T_p = 1$ , for scaled time  $T = t/t_{ref}$ .

In Fig. 6,  $\beta$  is set at 0.1, and  $\rho$  varies. In contrast, in Fig. 7 the product  $\rho\beta$  is considered to be a constant, specifically  $\rho\beta = 9$ , in keeping with an approximately constant Weibull shape parameter for strength. The value for  $\beta$  is then calculated based on the varying  $\rho$  value. This study focuses on the case  $\beta \leq 1$ .

Figure 6 shows that the models give remarkably similar results for large  $\rho$  values, with the differences between models becoming greater as  $\rho$  decreases. Increasing the proof ratio,  $\sigma_p/\bar{\sigma}$ , increases the conditional reliability in these models, assuming that  $\beta \leq 1$ . The CPL-W always provides a lower bound on instances of the 1979 functional form, and thus the CPL-W is the most conservative, of the models considered, in its conditional reliability predictions.

Figure 7 is very similar to Fig. 6, but shows that for a constant strength distribution, and thus a constant value of  $\rho\beta$ , as the value of  $\beta$  increases, the differences between the models increase. In contrast, if  $\rho\beta$  is allowed to vary, then as the value of  $\beta$  increases the differences between the models decrease as then the variability inherent in the material is being reduced. As before in Fig. 6, increasing the proof ratio increases the amount of difference between models.

To fully see how the conditional reliabilities relate across values of  $\sigma_p/\bar{\sigma}$  as well as to the original lifetime reliability, Fig. 8 plots reliabilities for the CPL-W model. In Fig. 8, the unconditional lifetime reliability is lowest, followed by the conditional reliabilities for increasing values of  $\sigma_p/\bar{\sigma}$ . These conditional reliabilities are also shown in Fig. 6, on separate axes.

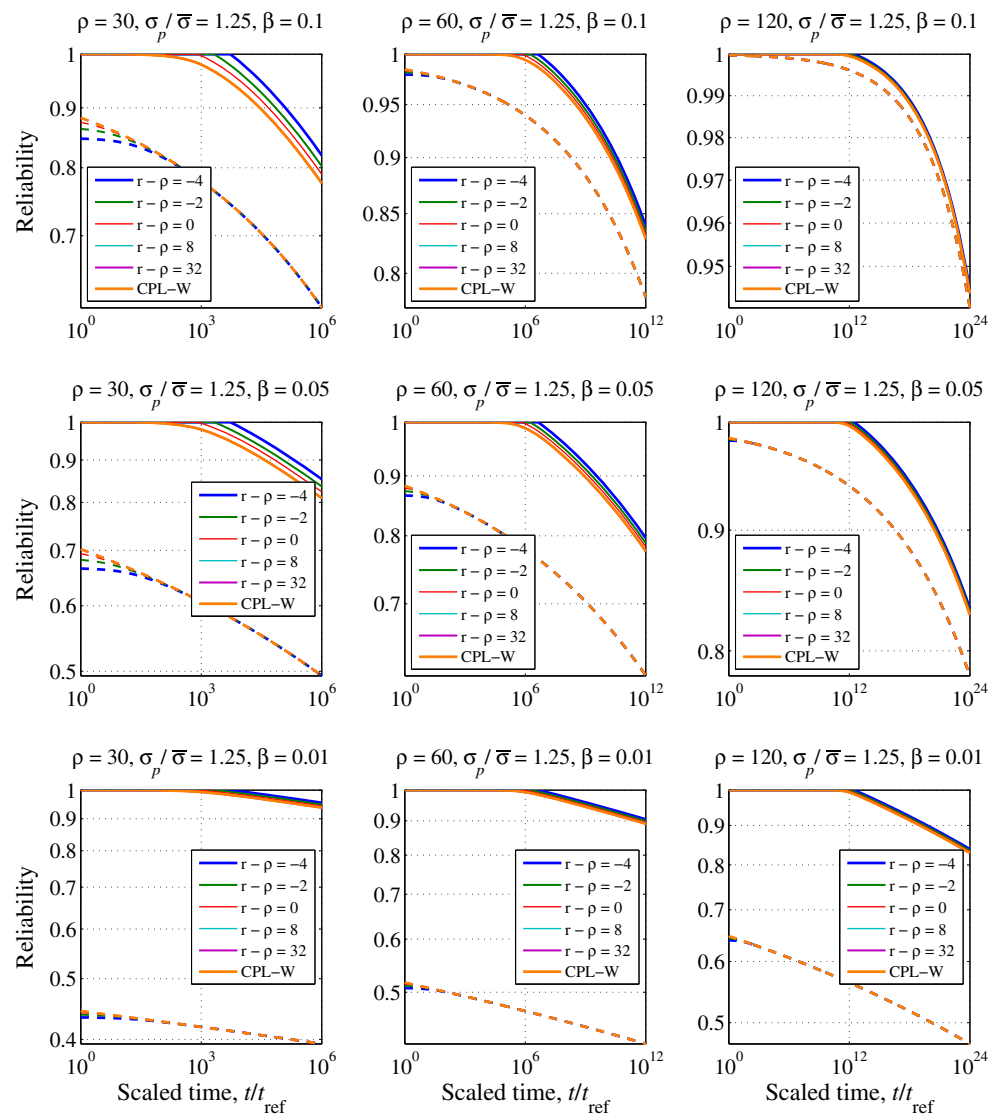
The difference between the reliability without a proof test vs. when  $\sigma_p/\bar{\sigma} = 1$  is that the second case is conditional on surviving the service load level,  $\bar{\sigma}$ , that might have been applied to a COPV before placement in a system, even if it was not a true proof test with  $\sigma_p > \bar{\sigma}$ .

In comparing the plots for long-term reliability, the conditional reliabilities are larger than or equal to the reliabilities for a constant lifetime load of  $\bar{\sigma}/\sigma_{ref} = 0.5$  (without a proof test). This can be seen in Fig. 8 in the particular case of the CPL-W model. This is further shown in Fig. 9 for  $\beta$  values of 0.1, 0.05 and 0.01, where the conditional reliability is shown with the solid lines and the reliability for a simple sustained load is shown in dashed lines.

For larger values of  $\beta$ , all of the models predict indistinguishable conditional reliabilities, as well as indistinguishable reliabilities under sustained loads (without proof testing). In the case where  $\beta > 1$ , as in composites using polymer fibers such as Kevlar, Vectran and Zylon, the conditional reliabilities and unconditional reliability for a simple sustained load may actually switch places, such that the conditional reliability is less than the sustained load reliability. However, carbon fibers are currently more widely used, due to their higher strength, and in carbon  $\beta \ll 1$ . In this case, the conditional reliabilities following a proof test are always higher than the sustained load reliabilities.

Figure 9 shows how the difference between the conditional reliability and the reliability for a sustained load increases as  $\beta$  decreases and as  $\rho$  increases, as seen before in Figs. 8 and 9. The effect of holding  $\rho\beta$  fixed and varying  $\rho$  can be seen by comparing the first two figures in the first row with the second two of the second row: the models become more similar as  $\rho$  is increased, holding  $\rho\beta$  fixed, the difference between the conditional reliabilities and the sustained lifetime reliabilities is similar, but the time scale over which the plots take place is doubled. Figure 9 also shows that the difference between the conditional reliability and the reliability for a sustained load also increases as  $\sigma_p/\bar{\sigma}$  increases, as expected.

**Figure 9** Plot of conditional reliabilities (47) and (49), in solid lines, and sustained lifetime reliabilities (17) and (29), in dashed lines, for varying values of  $\rho$  and  $\beta$ , where  $\bar{\sigma}/\sigma_{\text{ref}} = 0.5$ ,  $t_p/t_{\text{ref}} = T_p = 1$ , and  $\sigma_p/\bar{\sigma} = 1.25$ , for scaled time  $T = t/t_{\text{ref}}$ .



## Discussion

The 1979 functional form, its two particular instances, the crack-growth model and the strength decay model, and the CPL-W model (a limiting case of the 1979 functional form) are more similar than different. The differences between the models focus on the relationship between the strength distribution and the lifetime distribution, and the concept of a ‘safe time’ after a proof test.

Assuming the models, all have similar lifetime distributions, and thus the parameters  $\sigma_{\text{ref}}$ ,  $\rho$ ,  $\beta$ , and  $t_{\text{ref}}$  are consistent across the models, the strength distributions will differ slightly unless the parameter  $\rho$  happens to be quite high,  $> 100$ . These strength distributions can be collapsed onto one another by

choosing different values of the parameters depending on the model.

As mentioned earlier, experimental evidence shows that the observed strength increases with the loading rate. In some cases at extremely high loading rates, the loading rate effect diminishes, but this is not of practical interest for stress rupture since the transition stress level is always much higher than the stresses used in stress rupture experiments, not to mention in service.

The CPL-W model always shows this sensitivity. For the 1979 functional form models, in the case where  $t_{\text{ref}} \ll \sigma_{\text{ref}}/(R\rho)$ , all of the models show this sensitivity. Otherwise in Eq. (31), the last term will become dominated by the first term, which eventually eliminates the sensitivity to the loading rate.

Under a simple sustained load, the CPL-W model gives the most optimistic reliability, relative to the other models. In contrast, the CPL-W model gives the most conservative conditional reliability following a proof test. Furthermore, under a sustained load, instances of the 1979 functional form where the quantity  $r - \rho$  is more negative give the most conservative reliability, relative to the other models. In contrast, these instances of the 1979 functional form give the most optimistic conditional reliability following a proof test.

All instances of the 1979 functional form have a 'safe time' after a proof test—a time for which the conditional reliability is one. The CPL-W model, being the limit of the 1979 functional form, does not have a true 'safe time,' though it does have a decreased rate of failure. According to these models, the safe time can account for the entire desired service life of a specimen.

There is anecdotal evidence suggesting that for materials where  $\beta \ll 1$ , the conditional reliability after a proof test can quickly become lower than the reliability at a sustained load. While there is no literature experimentally determining the reliability after a proof test, there is enough concern about the possible damaging effects of proof testing to motivate new modeling approaches [11, 32]. Proof testing is known to do damage to the composite, through acoustic emission. After a proof test, there will be clusters of broken fibers that are larger than the clusters that would have been formed by loading just to the service load. These larger clusters create larger stress concentrations in the composite and act as possible sites for future failure. The damage done in a proof test may thus cancel out any benefits from weeding out weak vessels.

The concept that proof testing could reduce the reliability has great practical importance, yet it is not predicted by any of the models considered in this paper when  $\beta \ll 1$ , despite there being as many as five parameters. On the other hand, none of these models have a strong physical basis in the micromechanics of a composite structure. It is quite possible that all of the current models have shortcomings in predicting composite behavior for load profiles more complex than a sustained or linearly increasing load, or when an excessively high proof load is used.

Determining the conditional reliability after a proof test is an important question. Current models predict

only benefits from proof testing, yet they disagree on how much of a benefit. In reality, a proof testing at a high stress level runs the risk of breaking a lot of fibers, which ultimately cannot be good. For the models discussed however, either there is no safe time, or the safe time may encompass the entirety of service life. Either prediction may not be consistent with the experimental evidence.

## Conclusions

The models compared in this paper exhibit many similar characteristics. The only distinguishing differences between the models tend to be for unrealistic materials or in portions of the distribution where failure is unlikely for typical experimental sample sizes. While these models have a lot of flexibility, none of them allow for the possibility that a proof test may damage the composite through excessive fiber failure to the point where the conditional reliability decreases comparatively rapidly to values below that for a non-proof-tested specimen.

The current experimental data are not sufficient to determine which of these models may be most accurate. Furthermore, there is reason to believe that none of the models accurately predict composite reliability under complex load profiles such as proof tests. None of the models compared here are based in the micromechanics of a composite structure, and thus there is a need for a micromechanics inspired model to deal with the question of proof testing and, in the process, unintended fiber breakage.

## References

- [1] Phoenix SL (1979) The asymptotic distribution for the time to failure of a fiber bundle. *Adv Appl Probab* 11:153–187
- [2] Coleman BD (1956) Time dependence of mechanical breakdown phenomena. *J Appl Phys* 27:862–866
- [3] Coleman BD (1957) A stochastic process model for mechanical breakdown phenomena. *Trans Soc Rheol* 1:153–168
- [4] Coleman BD, Knox AG (1957) The interpretation of creep failure in textile fibers as a rate process. *Text Res J* 27:393–399

- [5] Coleman BD (1958) Time dependence of mechanical breakdown in bundles of fibers. III. The power law breakdown rule. *Trans Soc Rheol* 2:195–218
- [6] Coleman BD (1958) Statistics and time dependence of mechanical breakdown in fibers. *J Appl Phys* 29:968–983
- [7] Tobolsky A, Eyring H (1943) Mechanical properties of polymeric materials. *J Chem Phys* 11:125–134
- [8] Glasstone S, Laidler KJ, Eyring H (1941) *The theory of rate processes*. McGraw-Hill, New York
- [9] Kelly A, McCartney LN (1981) Failure by stress corrosion of bundles of fibres. *Proc R Soc Lond A* 374:1759
- [10] Christensen RM (1984) Interactive mechanical and chemical degradation in organic materials. *Int J Solids Struct* 20(8):791–804
- [11] Reeder J (2012) Composite stress rupture: a new reliability model based on strength decay. Report NASA/TM-2012-217566, L-20122, NF1676L-14234
- [12] Newman WI, Phoenix SL (2001) Time-dependent fiber bundles with local load sharing. *Phys Rev E* 63:021507
- [13] Phoenix SL, Newman WI (2009) Time-dependent fiber bundles with local load sharing. II. General Weibull fibers. *Phys Rev E* 80:066115
- [14] Christensen RM, Glaser RE (1985) Application of kinetic fracture mechanics to life prediction for polymeric materials. *J Appl Mech Trans ASME* 52(1):1–5
- [15] Glaser RE, Christensen RM, Chiao TT (1984) Theoretical relations between static strength and lifetime distributions for composites: an evaluation. *Compos Technol Rev* 6(4):164–167
- [16] Phoenix SL (2000) Modeling the statistical lifetime of glass fiber/polymer matrix composites in tension. *Compos Struct* 48(1):19–29. [https://doi.org/10.1016/S0263-8223\(99\)00069-0](https://doi.org/10.1016/S0263-8223(99)00069-0)
- [17] Phoenix SL, Grimes-Ledesma L, Thesken JC, Murthy PLN (2006) Reliability modeling of the stress-rupture performance of Kevlar 49/epoxy pressure vessels: revisiting a large body stress rupture data to develop new insights. In: 21st annual technical conference and proceedings American Society for composites, University of Michigan-Dearborn, Dearborn
- [18] Phoenix SL, Murthy PLN (2007) Pro's and cons of proof testing carbon composite overwrapped pressure vessels: a comparison of two mathematical models, AIAA Paper No. 2007–2325, presented at 48th AIAA/ASME/ASCE/AHS/ASC structures, structural dynamics, and materials conference, Honolulu
- [19] Phoenix SL (1978) The asymptotic time to failure of a mechanical system of parallel members. *SIAM J Appl Math* 34:227–246
- [20] Phoenix SL (1978) Stochastic strength and fatigue of fiber bundles. *Int J Fract* 14:327–344
- [21] Freudenthal AM (1973) Fatigue and fracture mechanics. *Eng Fract Mech* 2:403–414
- [22] Miner MA (1945) Cumulative damage in fatigue. *ASME J Appl Mech* 12(3):159–164
- [23] Taylor HM (1987) A model for the failure process of semicrystalline polymer materials under static fatigue. *Prob Eng Inf Sci* 1:133–162
- [24] Phoenix SL (1982) Statistical modeling of the time and temperature dependent failure of fibrous composites. In: *Proceedings of the 9th U.S. National congress of applied mechanics*. American Society of Mechanical Engineers
- [25] Phoenix SL, Kuo CC (1983) Recent advances in statistical and micromechanical modeling of time dependent failure of fibrous composites. 1983 *Advances in Aerospace Structures, Materials and Dynamics—AD-06 ASME Book No. H00272*
- [26] Tierney L-J (1984) A probability model for the time to fatigue failure of a fibrous composite with local load sharing. *Stoch Process Appl*. 18:1–14
- [27] Zhurkov SN (1965) Kinetic concept of the strength of solids. *Int J Fract Mech* 1:311–323
- [28] Wu HF, Phoenix SL, Schwartz P (1988) Temperature dependence of lifetime statistics for single Kevlar 49 filaments in creep-rupture. *J Mater Sci* 23:1851–1860. <https://doi.org/10.1007/BF01115731>
- [29] Phoenix SL, Tierney LJ (1983) A Statistical model for the time dependent failure of unidirectional composite materials under local elastic load-sharing among fibers. *Eng Fract Mech* 18:193–215
- [30] Engelbrecht-Wiggans A, Phoenix SL (2016) Comparison of maximum likelihood approaches for analysis of composite stress rupture data. *J Mater Sci* 51:6639–6661. <https://doi.org/10.1007/s10853-016-9950-3>
- [31] Reeder JR (2014) The inclusion of arbitrary load histories in the strength decay model for stress rupture. In: *Proceedings of the American society for composites—29th technical conference*, ASC 2014
- [32] Phoenix SL (1975) Statistical analysis of flaw strength spectra of high-modulus fibers. In: *Composite reliability*, ASTM STP 580. American Society for Testing and Materials, Philadelphia, Pennsylvania, pp 77–89